Sensors and Materials, Vol. 35, No. 1 (2023) 25–38
MYU Tokyo

S & M 3153

Diamagnetic-levitation-based Electromagnetic Energy Harvester for Ultralow-frequency Vibrations and Human Motions

Kun Zhang,[1,2*] Bo Zhang,[1,2] Wei Feng,[1,2]
Zongyao Liu,[1,2] Huipeng Shen,[1,2] and Baoguo Liu[1,2]

[1]Henan Key Laboratory of Super Hard Abrasives Grinding Equipment, Henan University of Technology, Zhengzhou 45001, China
[2]School of Electromechanical Engineering, Henan University of Technology, Zhengzhou 450001, China

(Received October 31, 2022; accepted December 28, 2022)

Keywords: diamagnetic levitation, ultralow frequency, bandwidth, vibration energy harvesting, electromagnetic induction

Converting ambient vibration energy into electrical energy is a potential technology for powering wireless sensor networks (WSNs). In this paper, an electromagnetic vibration energy harvester (EVEH) based on a diamagnetic levitation system is proposed for harvesting energy from ultralow-frequency, broadband vibration sources. In this design, a diamagnetic levitation structure is utilized to reduce the operating frequency, and mechanical impact is effectively introduced to broaden the working bandwidth. A simulation model of the energy harvester is built to illustrate the energy conversion process. The performance of the energy harvester is experimentally investigated under harmonic excitation with different acceleration levels and frequencies. At an acceleration of 1 g, a maximum peak-to-peak voltage of 370 mV is measured over a wide frequency range of 3–16 Hz, and the root mean square (RMS) output power at the optimal resistance is obtained as 26.7 μW at the excitation frequency of 6 Hz. In addition, the real-time characteristic of the proposed energy harvester is explored by harvesting energy from human motions such as hand shaking, stepping, and jumping. Compared with recent diamagnetic-levitation-based vibration energy harvesters, the harvester can be efficiently operated in an ultralow-frequency, random, and large-amplitude-vibration environment.

1. Introduction

With the advancement of microelectronics technology and wireless communication technology, wireless sensor networks (WSNs) are increasingly widely used in structural health monitoring, smart agriculture, environmental protection, national security, and other fields.(1) Generally, WSN nodes are powered by a chemical battery, such as a lithium battery. However, chemical batteries have a short lifespan and require replacement and maintenance, which may cause WSN nodes to be unable to operate stably for long periods, and even lead to the paralysis of the entire WSN network. Fortunately, the ambient environment contains abundant energy

*Corresponding author: e-mail: kunzhang@haut.edu.cn
https://doi.org/10.18494/SAM4202

ISSN 0914-4935

sources, such as thermal, solar, vibration, and RF, which can be converted into electricity to power WSN nodes.[2] Among them, vibration energy is particularly attractive owing to its ubiquitous existence and abundant availability. Therefore, harvesting vibration energy from the ambient environment is an ideal solution for a sustainable power supply.[3]

Currently, vibration energy harvesting mainly makes use of three common mechanisms: piezoelectric,[4,5] electrostatic,[6,7] and electromagnetic.[8,9] Electromagnetic vibration energy harvesters (EVEHs) have attracted extensive attention from researchers owing to their high output current, low internal resistance, and simple structure. Most traditional EVEHs are designed to achieve optimal performance only when the resonance frequency matches the ambient vibration frequency. However, the ambient vibration frequency varies randomly in a wide range, meaning that the EVEH cannot effectively harvest the ambient vibration energy. Therefore, it is necessary to broaden the operating bandwidth of EVEHs for practical applications. To achieve this, researchers have proposed various bandwidth-broadening methods including monostable,[10,11] multistable,[12,13] multimodal,[14,15] multi-degree-of-freedom,[16,17] and impact methods.[18,19] Although these methods broaden the working bandwidth, the improved harvesters cannot effectively scavenge energy from ambient vibration sources with ultralow frequency, such as human motion and wave heave motion, in which frequency is usually lower than 10 Hz.[20,21]

In recent years, considerable attention has been paid to diamagnetic-levitation-based EVEHs consisting of a diamagnetic levitation system and an electromagnetic transduction mechanism. A diamagnetic levitation system[22] composed of diamagnetic materials and permanent magnets has the advantages of no friction, low damping, and low stiffness,[23,24] which are beneficial to improving the performance of EVEHs to obtain low-frequency vibration energy. Palagummi *et al.*[25] proposed a monostable EVEH based on a vertical diamagnetic levitation structure that generated a root mean square (RMS) output power of 1.72 μW at 2.1 Hz. Gao *et al.*[26] designed a bistable EVEH using a horizontal diamagnetic levitation mechanism, which obtained a peak power of 333.7 μW at a vibration level of 0.6 m/s^2 over a range of 0.5–4.5 Hz. Zhang *et al.*[27] reported a low-frequency wideband piecewise linear EVEH based on the diamagnetic levitation mechanism, in which a floating magnet impacts an elastic film at the edge under low-frequency horizontal vibration excitation. Cheng *et al.*[28] designed a monostable diamagnetic levitation EVEH using the Taguchi method, which generated an RMS voltage of 250.69 mV and a power of 86.8 μW under 2.6 Hz vibration excitation.

In this paper, we present a mechanical-impact-driven EVEH based on the diamagnetic levitation system, which consists of planar copper coils and a diamagnetic levitation structure containing a floating magnet. The main characteristic of the device makes it particularly suitable for use with ultralow-frequency, broadband vibration sources. The work reported in this paper is organized as follows. Following the introduction, Sect. 2 describes the design of the device and its working principle. The theories of diamagnetic levitation and energy conversion are given in Sect. 3, together with the modeling of the EVEH and simulation analysis. The experimental setup, detailed tests, and a comparison with previous studies are described in Sect. 4. Conclusions are drawn in Sect. 5.

2. Design Structure and Working Principle

Figure 1 shows a schematic of the proposed EVEH, which consists of a floating magnet, a fixed magnet, two highly oriented pyrolytic graphite (HOPG) sheets, four planar copper coils, and an adjustable shell. The floating magnet is levitated between the two HOPG sheets, and the fixed magnet is located above the upper HOPG sheet. The two magnets are magnetized axially in the same direction and attract each other. At the same time, HOPG sheets generate magnetic repulsion forces on the floating magnet. When the forces acting on the floating magnet are balanced, the floating magnet will achieve a stable levitation state without external disturbance. The four planar coils are divided into two groups and fixed on the opposite inner sides of the two HOPG sheets. Under vertical vibration excitation, the floating magnet is forced to vibrate along the axial direction of the floating magnet, and when the displacement of the floating magnet exceeds the levitation gap d, the floating magnet impacts the coils, and its instantaneous velocity changes rapidly. Meanwhile, the magnetic flux through the coils changes continuously with the motion of the floating magnet, which results in an induced voltage across the coils, then the mechanical vibration energy is converted into electric energy.

3. Theoretical Model and Analysis

3.1 Diamagnetic levitation principle

A diamagnetic material is a magnetic medium whose magnetic susceptibility is less than zero, which means that a reversed induced magnetic field is generated when a diamagnetic

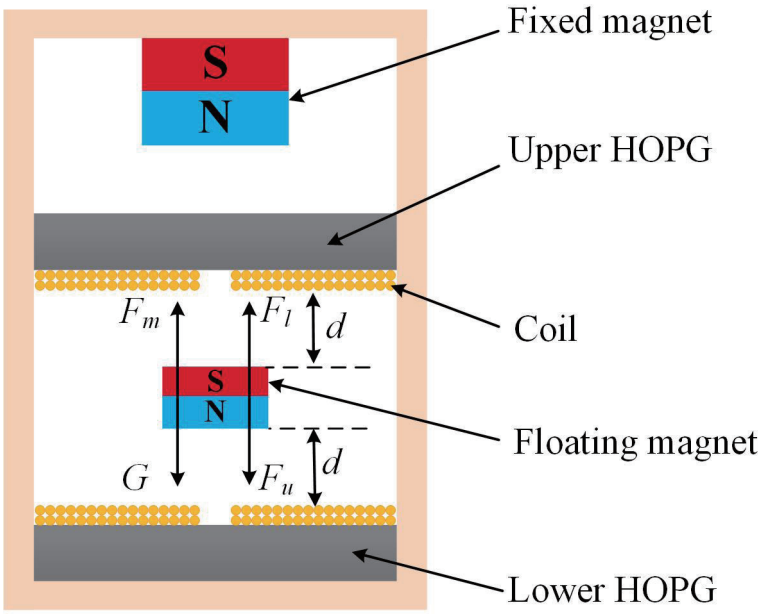

Fig. 1. (Color online) Schematic of proposed EVEH and force analysis of floating magnet.

material is placed in an external magnetic field. A repulsive force is produced between the two opposing magnetic fields, which is known as a diamagnetic force and can be expressed as [29]

$$dF = -\nabla\left(M \cdot B\right)dv, \tag{1}$$

where M is the magnetization vector of the diamagnetic material and B is the magnetic field vector of the external magnetic field.

Since HOPG is an anisotropic material, the magnetization can be determined as

$$M = \frac{\chi_x}{\mu_0} B_x \vec{i} + \frac{\chi_y}{\mu_0} B_y \vec{j} + \frac{\chi_z}{\mu_0} B_z \vec{k}, \tag{2}$$

where Bx, By, and Bz are the components of the external magnetic field along the x-axis, y-axis, and z-axis, and χ_x, χ_y, and χ_y represent the magnetic susceptibilities of the HOPG in the three directions, respectively.

By integrating over the whole volume V of the diamagnetic material, the diamagnetic force can be written as

$$F = -\iiint_V \left(\frac{\chi_x}{\mu_0} B_x \frac{\partial B_x}{\partial x} + \frac{\chi_y}{\mu_0} B_y \frac{\partial B_y}{\partial y} + \frac{\chi_z}{\mu_0} B_z \frac{\partial B_z}{\partial z} \right) dv. \tag{3}$$

An attractive magnetic force is formed between two cylindrical magnets with the same magnetization direction, which can be given as follows:

$$F_m = \frac{\mu_r - 1}{2\mu_0 \mu_r} \iint_s B^2 ds, \tag{4}$$

where B is the magnetic induction intensity at the location of the floating magnet, $\mu_0 = 4\pi \times 10^{-7}$ is the permeability of vacuum, μ_r is the relative magnetic permeability, and S is the surface area of the floating magnet.

Therefore, the floating magnet is attracted by the magnetic force from the fixed magnet and is repelled by the two repulsive forces from the two HOPG sheets in the device. Figure 1 shows the force analysis of the floating magnet. Under the combined action of F_m, F_u, F_l, and gravity, the floating magnet can realize stable levitation at a certain position, which can be expressed as follows:

$$F_m + F_l - F_u - G = 0, \tag{5}$$

where F_m is the magnetic attractive force between the floating magnet and the fixed magnet, G is the gravity of the floating magnet, and F_u and F_l are the repulsive forces of the upper HOPG sheet and the lower HOPG sheet acting on the floating magnet, respectively.

3.2 Energy conversion analysis

By considering the working principle, the proposed EVEH can be simplified to a single-degree-of-freedom impact oscillator coupled with an electric circuit, as shown in Fig. 2. The governing equations of the floating magnet can be given by[30]

$$\begin{cases} m\ddot{z} + c\dot{z} + F_r(z) + F_L\left(i,\dot{z}\right) = mA\omega^2 \sin\left(\omega t\right), \\ \dot{z}_+ = -\eta \dot{z}_- \qquad\qquad \text{when } \left|z\right| = \Delta, \\ \dot{i}L_{coil} + i\left(R_{load} + R_{coil}\right) = V(z,\dot{z}), \end{cases} \tag{6}$$

where m is the mass of the floating magnet, c is the mechanical damping coefficient, F_r is the restoring force of the floating magnet in the z-direction, F_L is the electromagnetic damping force, z is the relative displacement of the floating magnet under harmonic excitation ($A\omega^2\sin\omega t$), Δ is the impact clearance, which is equal to the levitation gap d of the floating magnet, R_{coil} is the internal resistance of the induction coil, R_{load} is the external load, L_{coil} is the inductance of the coil, and V is the induced voltage. $\dot{z}_-$ and $\dot{z}_+$ are the instantaneous velocities before and after the collision, respectively. η is the restitution coefficient of the instantaneous velocities during the collision.

By ignoring the influence of the induced magnetic field generated by the HOPG sheet, the induced voltage across the coil can be determined using Faraday's law of electromagnetic induction, which can be expressed as

$$V\left(z,\dot{z}\right) = -\frac{d\varphi}{dt} = -\frac{d\varphi}{dt}\frac{dz}{dt} = -2\pi\dot{z}\sum_{r_{coil}=r_{in}}^{r_{coil}=r_{out}}\int_0^{r_{coil}} B\left(z,r\right)rdr, \tag{7}$$

where φ is the magnetic flux across the coil, B is the magnet field generated by the floating magnet, and r_{in} and r_{out} are the inner and outer radii of the coils, respectively.

In addition, the energy conversion between the mechanical and electrical systems can be written as

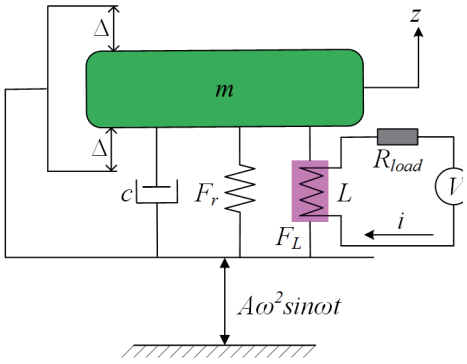

Fig. 2. (Color online) Simplified model of proposed EVEH.

$$F_L\left(i,\dot{z}\right)\dot{z} = iV\left(z,\dot{z}\right). \tag{8}$$

The electrical energy output of the energy harvester can be obtained using Eqs. (6)–(8). When the EVEH works in an open-circuit situation, there is no electromagnetic damping force in the energy harvesting system.

3.3 Numerical calculation and analysis

As shown in Fig. 3, we built a Simulink simulation model of the proposed device based on the system parameters listed in Table 1 to understand the energy conversion process. To run this model, it is necessary to obtain the resultant force of the floating magnet and the magnetic flux

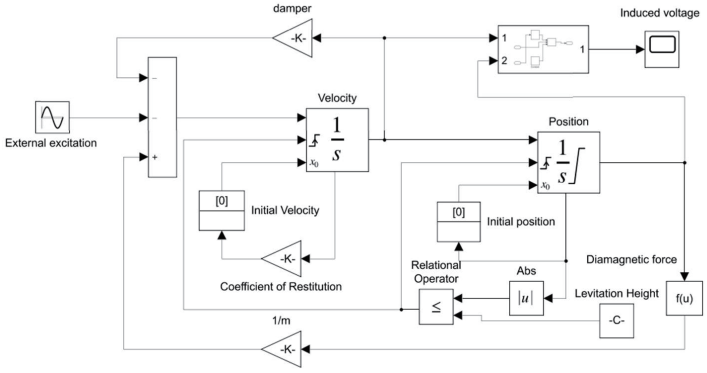

Fig. 3. Simulink model of proposed EVEH.

Table 1
Material properties and structure parameters used in simulation model and experimental prototype.

	Parameter	Value
Planar coil	Size (mm)	Φ28 × Φ5 × 0.09
	Turns	65
	Material	Copper
	Number	4
	Internal resistance	12.5 Ω
Floating magnet	Diameter (mm)	12
	Thickness (mm)	4
	Material	NdFeB grade 52
	Remanent magnetization (T)	1.47
Fixed magnet	Diameter (mm)	12.7
	Thickness (mm)	6.35
	Material	NdFeB grade 52
	Remanent magnetization (T)	1.32
HOPG sheet	Diameter (mm)	28
	Thickness (mm)	5
	Magnetic susceptibility $\chi_{\perp}$	-450×10^{-6}
	Magnetic susceptibility $\chi_{\parallel}$	-85×10^{-6}

through the induction coil at each relative position. The variation of the resultant force of the floating magnet with its displacement is determined numerically with the distance between the two HOPG sheets set to 6 mm, as shown in Fig. 4. The obtained curve can be fitted to the nonlinear function

$$F = -888400x^3 + 127.8x^2 - 0.05095x + 0.000005174. \quad (9)$$

The magnetic flux through a planar coil is obtained by the FEM software COMSOL Multiphysics 5.5. Figure 5 shows the obtained magnetic flux through the planar coil as a function of the distance z between the coil and the floating magnet. The magnetic flux decreases with increasing distance, and the following quadratic function is used to fit the obtained curve:

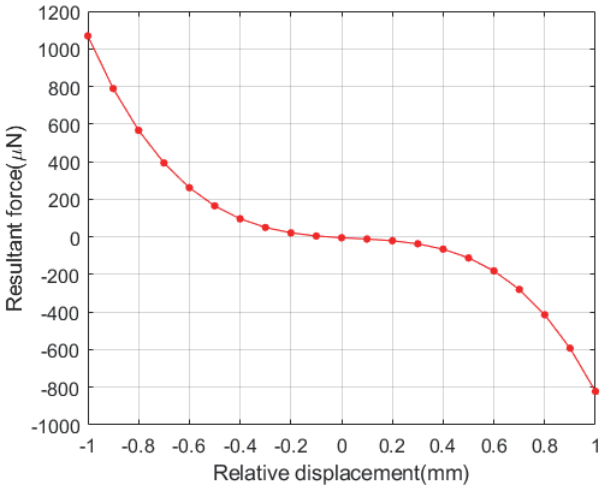

Fig. 4. (Color online) Resultant force versus relative displacement of floating magnet.

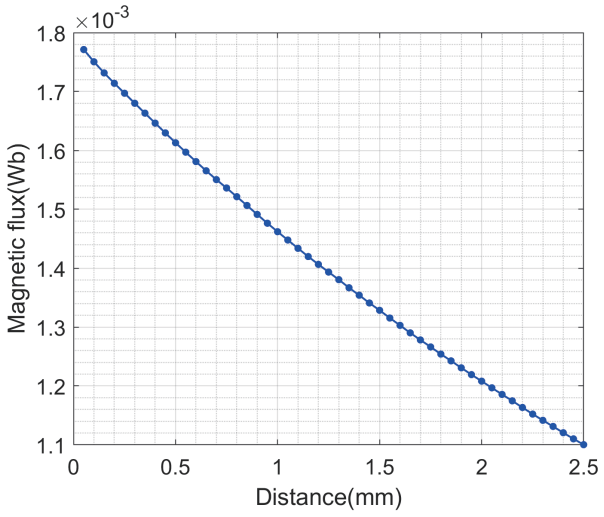

Fig. 5. (Color online) Trend of magnetic flux with distance between induction coil and floating magnet.

$$\Phi = 31.82z^2 - 0.3517z + 0.001783. \tag{10}$$

Figure 6 shows the relative displacement of the floating magnet and the induced voltage under external excitation with a frequency of 10 Hz and an acceleration of 0.5 *g*. As shown by the curve of the relative displacement, there are three impacts, numbered in the figure, between the floating magnet and the lower HOPG sheet in one cycle, because the dynamic response of the floating magnet is not synchronized with the external excitation. When the floating magnet impacts the HOPG sheet, the velocity of the floating magnet changes abruptly, resulting in a sudden change in the induced voltage. The induced voltage reaches a maximum negative value at the first impact and a maximum positive value at the second impact motion, because the relative displacement of the floating magnet reaches 2 mm before the first two impacts.

4. Experiments and Discussion

4.1 Experimental test system

To further explore the output performance of the proposed EVEH, a prototype based on the structure parameters in Table 1 is manufactured. As shown in Fig. 7, the main structure is fabricated by 3D printing technology using a high-strength ABS material. Two HOPG sheets are first cut into a cylindrical shape by micro-electric discharge machines, then finely polished to the desired size. Four planar coils of enameled copper wire of 0.09 mm diameter are wound in a spiral.

Meanwhile, an energy harvester test bench is developed as shown in Fig. 7. On this test bench, a cylindrical acrylic plate is fixed on the post rod of a shaker (SA JZ010), which serves as a stage on which to mount the accelerometer (PCB 052C03) and the prototype. The vibration excitation signal is generated by a function generator (RIGOL DG1022) and amplified by a 200 W power amplifier (SA PA020) to regulate the frequency and amplitude of the shaker. The

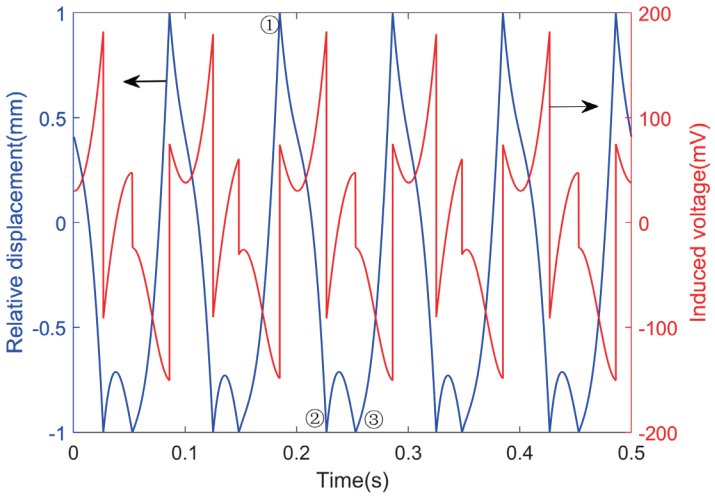

Fig. 6. (Color online) Simulated relative displacement and induced voltage under 10 Hz, 0.5 *g* vibration excitation.

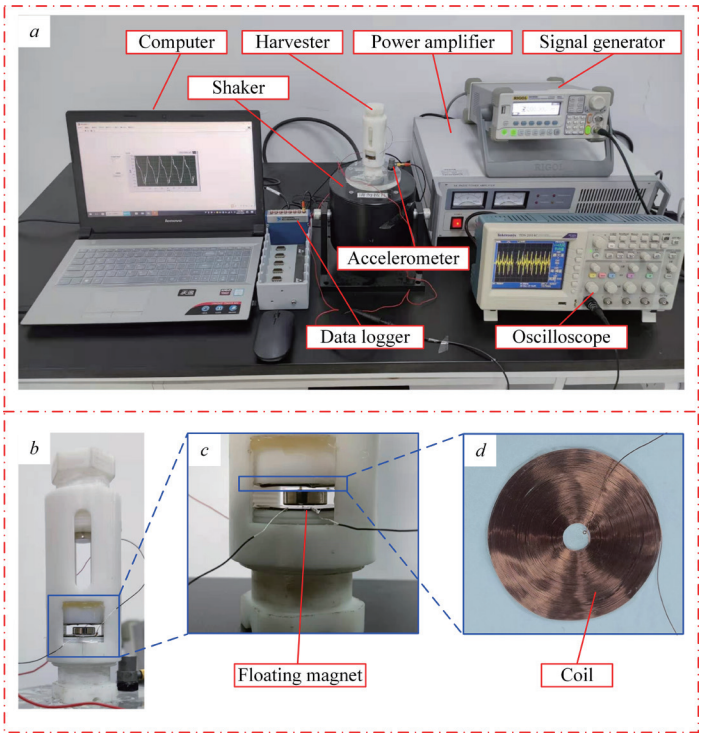

Fig. 7. (Color online) Experimental setup for testing electric energy output characteristics of the proposed EVEH.

accelerator is used to monitor the vibration level of the shaker, and the monitoring signal is transmitted to a visual monitoring platform programmed by LabVIEW through a DAQ card (NI 9231). The output voltage of the energy harvester is measured and recorded by an oscilloscope (Tektronix TDS2014C).

4.2 Experimental results under harmonic excitation

The performance of the proposed EVEH is tested under harmonic excitation using the above experimental setup. The open-circuit peak-to-peak voltage of the EVEH prototype measured experimentally under excitation accelerations of 0.6, 0.8, and 1.0 g is depicted in Fig. 8. During the experiment, the gap between the HOPG sheet and the floating gap is set to 1.0 mm. Since the shaker cannot generate good harmonic excitation at frequencies below 3 Hz, the experiment is carried out in the frequency range of 3–25 Hz. Within the defined frequency domain, the peak-to-peak voltage response has two peaks. Under the three excitation accelerations, the peak-to-peak voltage reaches its first peak at a frequency of 7 Hz, which is caused by the multi-degree-of-freedom system with multiple frequency components composed of the energy harvester, the frame, and the shaker. Moreover, the magnitude of the first peak increases with increasing excitation acceleration. Then, the peak-to-peak voltage reaches its second peak as the frequency increases. At this point, the peak-to-peak voltage reaches its maximum value, but the peak value and the corresponding excitation frequency vary with the excitation acceleration. At the excitation accelerations of 0.6, 0.8, and 1.0 *g*, the energy harvester generates maximum peak-to-peak voltages of 280, 315, and 370 mV at 14, 15, and 16 Hz and its operating bandwidths are

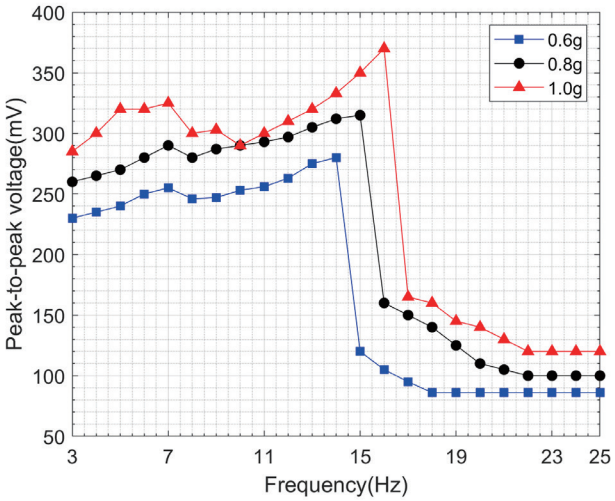

Fig. 8. (Color online) Measured peak-to-peak voltage of the EVEH prototype against operating frequency under excitation accelerations of 0.6, 0.8, and 1.0 g.

approximately 11, 12, and 13 Hz, respectively. With a further increase in the excitation frequency, the frequency response of the energy harvester suddenly drops, which is called the jump phenomenon and is caused by the nonlinear vibration of the energy harvester system. After the sudden drop, the peak-to-peak voltage decreases gradually with increasing excitation frequency. On the whole, the peak-to-peak voltage tends to increase with the excitation acceleration. This is because an increase in the excitation acceleration increases the energy input of the energy harvester.

Figure 9 shows the peak-to-peak voltage against the load resistance and the power delivered to the load resistance. The peak-to-peak load voltages and output power are measured by varying the load resistance under different excitation accelerations at the excitation frequency of 6 Hz. The measured results indicate that with increasing load resistance, the peak-to-peak load voltage increases gradually, whereas the power first increases and then decreases. The maximum output power of the energy harvester prototype can be obtained when the load resistance matches the internal resistance of the induction coils (which is 50 Ω). When the excitation accelerations are 0.2, 0.3, and 0.5 g, the maximum output powers of the prototype are 11.6, 15.3, and 26.7 μW, respectively.

4.3 Experimental results under human motion

The proposed EVEH is also characterized under realistic human motion excitations, including hand shaking, stepping, and jumping, as shown in Fig. 10. In the experiment, the human motion serves as an ultralow-frequency excitation source, the induced voltage of the energy harvester is measured by an oscilloscope, and the excitation acceleration generated by each human motion is acquired by an acceleration sensor connected with a DAQ card. In addition, the excitation frequency spectrum is obtained by a fast Fourier transform. Figure 11

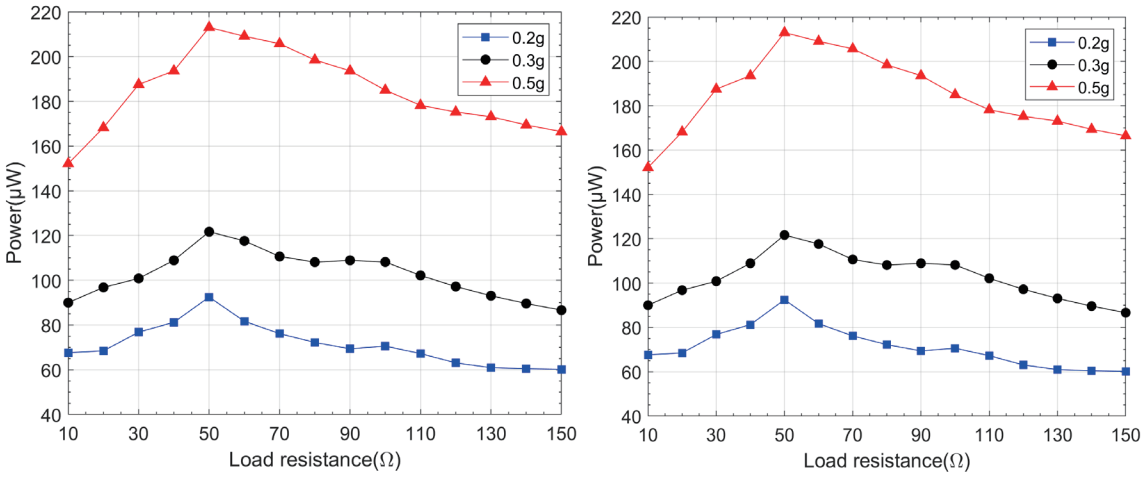

Fig. 9. (Color online) Measured output voltage and power of the prototype plotted against load resistance at the excitation frequency of 6 Hz under different excitation accelerations: (a) peak-to-peak voltage and (b) RMS power.

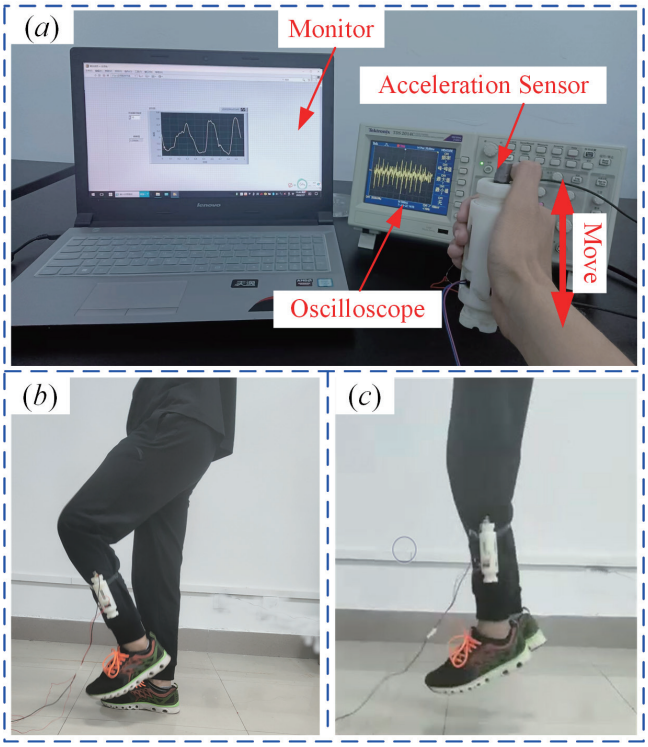

Fig. 10. (Color online) EVEH prototype excited by different human motions: (a) hand shaking, (b) stepping, and (c) jumping.

shows the induced voltage of the energy harvester, the excitation acceleration, and the excitation frequency spectrum under different human motions. It can be seen from Fig. 11(a) that the maximum induced voltage for vertical human shaking with 0.83 *g* excitation acceleration and 3.6

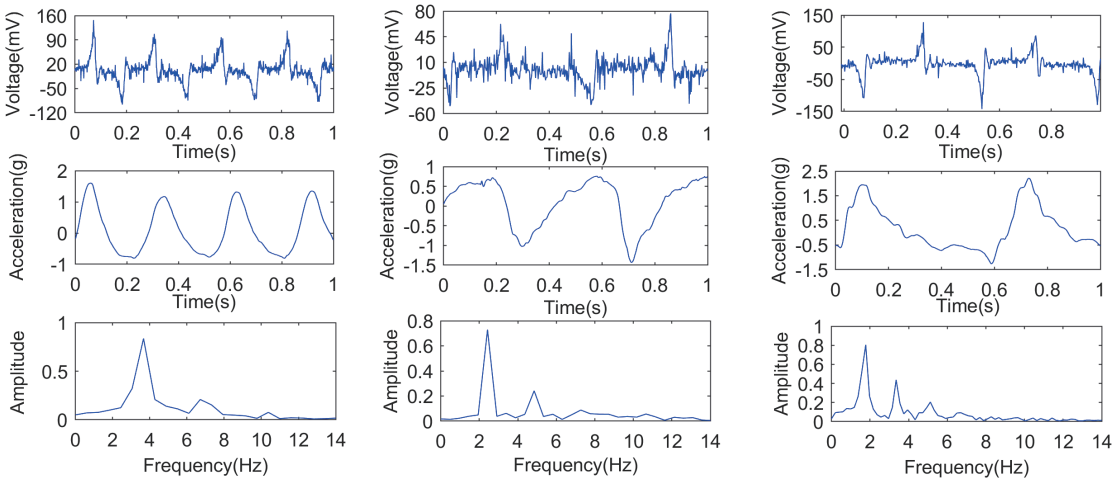

Fig. 11. (Color online) Voltage response, excitation acceleration, and excitation frequency spectra for EVEH prototype driven by human motion: (a) hand shaking, (b) stepping, and (c) jumping.

Hz frequency is 147.2 mV. In the other two experiments, the EVEH prototype is vertically attached to a human lower limb, as shown in Figs. 10(b)–10(c). The maximum induced voltage of the energy harvester is 76.8 mV under the jumping motion with 0.73 *g* excitation acceleration and 2.4 Hz frequency, which can reach up to 142.4 mV under the jumping motion with 0.8 *g* excitation acceleration and 1.77 Hz frequency. Note that the acceleration and frequency are similar in the two motions, but the maximum induced voltage is clearly different. This is mainly because the prototype does not always remain vertical during the stepping motion. Therefore, it can be concluded that the excitation angle affects the performance of the EVEH. The interaction between the excitation angle and the power output will be discussed in future work. In addition, a human motion test verified that the energy harvester remains effective for vibration frequencies of below 3 Hz.

4.4 Performance comparison

A comparison between the proposed EVEH and other EVEHs using diamagnetic levitation is given in Table 2, which summarizes the optimal performance and corresponding working conditions of diamagnetic-levitation-based vibration energy harvesters. Note that both horizontal and vertical diamagnetic levitation structures have been adopted to develop EVEHs. The axis of the floating magnet in the horizontal (vertical) diamagnetic levitation structure is horizontal (vertical). As shown in Table 2, the proposed harvester does not have a high output power but has an outstanding frequency bandwidth and can withstand vibration excitation with a large acceleration amplitude, which means that the proposed EVEH is more efficient than other EVEHs in harvesting low-frequency, random environmental vibration energy.

Table 2
Performance comparison of different EVEHs using diamagnetic levitation.

Reference	Frequency (Hz)	Acceleration (m/s^2)	Power (μW)	Bandwidth (Hz)	Structure type	Excitation direction
Palagummi *et al.*[25]	2.1	0.081	1.72	<1.0	Vertical	Vertical
Gao *et al.*[26]	3.0	0.6	333.7	2.0	Horizontal	Vertical
Su *et al.*[27]	5.0	7.86	152	3.0	Vertical	Horizontal
Palagummi *et al.*[31]	1.2	0.0434	3.6	<1.0	Horizontal	Vertical
Palagummi *et al.*[32]	1.9	0.0546	9.47	<1.0	Horizontal	Vertical
Palagummi *et al.*[33]	5.8	1.99	60.6	2.2	Horizontal	Vertical
This work	16	9.8	26.7	>13	Vertical	Vertical

5. Conclusion

In this work, an ultralow-frequency, broadband EVEH is proposed, which couples with a diamagnetic levitation mechanism and a mechanical impact mechanism. The electromechanical model of the proposed EVEH is built as a single-degree-of-freedom damped vibration system with limited amplitude. Multiple impacts in one cycle are detected by simulation analysis. An experimental prototype is constructed and tested under different excitation accelerations and frequencies. The results show that the induced voltage and output power increase with the excitation acceleration. When the EVEH is excited by an excitation acceleration of 1 *g*, the maximum peak-to-peak voltage can reach 370 mV in the frequency range of 3–16 Hz, and the RMS output power across a 50 Ω optimum load resistance is 26.7 μW at the frequency of 6 Hz. Experimental results for different human motions illustrate that the harvester remains effective for harvesting vibration energy at frequencies lower than 3 Hz. Compared with previously designed diamagnetic-levitation-based energy harvesters, the proposed harvester can respond to random and large-amplitude vibration excitation. It is particularly suitable for working in ultralow-frequency, large amplitude, and random vibration environments.

Acknowledgments

This work was supported by the National Natural Science Foundation of China (12072106 and 52005166), the Key Scientific and Technological Project of Henan Province (202102210288 and 212102210618), the Research Foundation for Advanced Talents of Henan University of Technology (2019BS054), Fundamental Research Funds for Henan Provincial Colleges and Universities in Henan University of Technology (2018QNJH04), and the Cultivation Programme for Young Backbone Teachers in Henan University of Technology (202221420191).

References

1 M. Gao, P. Wang, Y. Cao, R. Chen, and D. Cai: IEEE Trans. Intell. Transp. Syst. **18** (2017) 1596.
2 F. K. Shaikh and S. Zeadally: Renewable Sustainable Energy Rev. **55** (2016) 1041.
3 T. Yildirim, M. H. Ghayesh, W. Li, and G. Alici: Renewable Sustainable Energy Rev. **71** (2017) 435.
4 X. Chen, X. Zhang, L. Chen, Y. Guo, and F. Zhu: Micromachines **12** (2021) 995.
5 E. Fakeih, A. S. Almansouri, J. Kosel, M. I. Younis, and K. N. Salama: Adv. Eng. Mater. **23** (2021) 2001364.

6 Z. Yang, L. Tang, K. Tao, K.C. Aw: Int. J. Precis. Eng. Manuf.-Green Technol. **8** (2021) 113.
7 Y. Naito and K. Uenishi: Sensors **19** (2019) 890.
8 C. M. Saravia: Mech. Syst. Signal Proc. **136** (2020) 106027.
9 Y. Shen and K. Lu: Energy Conv. Manag. **222** (2020) 113233.
10 K. Fan, M. Cai, H. Liu, and Y. Zhang: Energy **169** (2019) 356.
11 W. Wang, J. Cao, D. Mallick, S. Roy, and J. Lin: Mech. Syst. Signal Proc. **108** (2018) 252.
12 M. A. Abdelnaby and M. Arafa: J. Braz. Soc. Mech. Sci. Eng. **42** (2020) 520.
13 M. Gao, Y. Wang, Y. Wang, and P. Wang: Appl. Energy **220** (2018) 856.
14 R. M. Toyabur, M. Salauddin, H. Cho, and J. Y. Park: Energy Conv. Manag. **168** (2018) 454.
15 V. J. Caetano and M. A. Savi: J. Intell. Mater. Syst. Struct. **32** (2021) 2505.
16 K. Fan, Y. Zhang, H. Liu, M. Cai, and Q. Tan: Renewable Energy **138** (2019) 292.
17 N. Yu, H. Ma, C. Wu, G. Yu, and B. Yan: Mech. Syst. Signal Proc. **156** (2021) 107608.
18 K. Ashraf, M. H. Md Khir, J. O. Dennis, and Z. Baharudin: Smart Mater. Struct. **22** (2013) 25018.
19 H. Zhang, S. Jiang, and X. He: Appl. Phys. Lett. **110** (2017) 223902.
20 H. Liu, C. Hou, J. Lin, Y. Li, Q. Shi, T. Chen, L. Sun, and C. Lee: Appl. Phys. Lett. **113** (2018) 203901.
21 W. Wang, J. Cao, N. Zhang, J. Lin, and W. Liao: Energy Conv. Manag. **132** (2017) 189.
22 Q. Wang, X. Ren, S. Jiao, X. Lei, S. Zhang, H. Liu, P. Luo, and L. Tu: Sens. Actuators, A **312** (2020) 112122.
23 S. Clara, H. Antlinger, A. Abdallah, E. Reichel, W. Hilber, and B. Jakoby: Sens. Actuators, A **248** (2016) 46.
24 L. Liu and F. G. Yuan: J. Sound Vibr. **332** (2013) 455.
25 S. Palagummi and F. G. Yuan: J. Sound Vibr. **342** (2015) 330.
26 Q. Gao, W. Zhang, H. Zou, W. Li, Z. Peng, and G. Meng: IEEE Trans. Magn. **53** (2017) 1.
27 K. Zhang, Y. Su, J. Ding, and Z. Duan: Appl. Phys. A **125** (2019).
28 S. Cheng, X. Li, Y. Wang, and Y. Su: Micromachines **12** (2021) 982.
29 T. H. Boyer: Am. J. Phys. **8** (1987) 688.
30 F. Khan, F. Sassani, B. Stoeber: J. Micromech. Microeng. **20** (2010) 125006.
31 S. Palagummi, J. Zou, and F. G. Yuan: J. Vib. Acoust. **137** (2015) 743.
32 S. V. Palagummi and F. G. Yuan: J. Intell. Mater. Syst. Struct. **28** (2016) 578.
33 S. Palagummi and F. G. Yuan: Sens. Actuators, A **279** (2018) 743.